

# Swing-Structured Triboelectric–Electromagnetic Hybridized Nanogenerator for Breeze Wind Energy Harvesting

Pinjing Lu, Hao Pang, Jie Ren, Yawei Feng, Jie An, Xi Liang, Tao Jiang,\*  
and Zhong Lin Wang\*

Wind energy is one of the most promising renewable energy sources, but harvesting low frequency breeze wind energy is hardly achieved using traditional electromagnetic generators (EMGs). Triboelectric nanogenerators (TENGs) provide a new approach for large-scale collection of distributed breeze wind energy (usually  $3.4\text{--}5.4\text{ m s}^{-1}$ ). Herein, by coupling the TENG and EMG, a swing-structured hybrid nanogenerator with improved performance and durability is designed. The dielectric brush and air gap designs can minimize the material wear and continuously supply the tribo-charges. Under external triggering, systematic comparisons are made about the output characteristics of TENG and EMG. The rectified peak power and average power of TENG are respectively, 60 and 635 times higher than those of EMG at moderate coil turn numbers, showing that TENG is much more effective than EMG for harvesting low-frequency distributed energy (high entropy energy). Furthermore, the hybrid nanogenerator and array device are hung on tree branches to demonstrate the effective harvesting of breeze wind energy, delivering total rectified peak power densities of  $2.07$  and  $1.94\text{ W m}^{-3}$  for single and array devices, respectively. The applications of powering portable electronics reveal the huge prospects of hybrid nanogenerator in self-powered environmental monitoring toward forest/park fire warning systems.

environmental pollution problems.<sup>[3,4]</sup> Under such circumstances, it is desirable to search for new clean and renewable energy sources from our environment, such as widely distributed wind energy in nature.<sup>[5]</sup> Harvesting wind energy has attracted increasing attention in the past decades.<sup>[6]</sup> Nowadays, the main way to exploit the wind energy is to drive the wind turbine blades to rotate by the wind force, converting the wind energy into mechanical energy, and then drive the electromagnetic generator (EMG) to generate electricity through the speed-increase gearbox.<sup>[7]</sup> Due to the technology limitations, it is rather challenging to collect irregular, random, and low-speed wind energy by using the EMG, with the main drawbacks of complex structure, large volume, and low energy conversion efficiency.<sup>[8,9]</sup> However, the emerging triboelectric nanogenerator (TENG) provides a new strategy for the efficient utilization of breeze wind energy.<sup>[10]</sup>

The TENG, also called as Wang generator, is a powerful mechanical energy harvesting technology, based on the coupling of triboelectrification and electrostatic induction.<sup>[11,12]</sup> Due to its fundamental mechanism of Maxwell's displacement current, it exhibits obvious advantage over the EMG at low frequency.<sup>[13,14]</sup> And, the TENG technology has been widely applied to scavenge the

## 1. Introduction

Energy is one of the most important resources that mark the quality of human life.<sup>[1,2]</sup> Continuous consumption of traditional fossil fuels has caused serious energy crisis and

P. Lu, H. Pang, Prof. T. Jiang  
Center on Nanoenergy Research  
School of Physical Science and Technology  
Guangxi University  
Nanning, Guangxi 530004, P. R. China  
E-mail: jiangtao@binn.cas.cn

P. Lu, H. Pang, J. Ren, Y. Feng, J. An, X. Liang, Prof. T. Jiang,  
Prof. Z. L. Wang  
CAS Center for Excellence in Nanoscience  
Beijing Key Laboratory of Micro-Nano Energy and Sensor  
Beijing Institute of Nanoenergy and Nanosystems  
Chinese Academy of Sciences  
Beijing 101400, P. R. China  
E-mail: zlwang@gatech.edu

J. Ren  
Beijing Key Laboratory of Printing and Packaging Materials  
and Technology  
Beijing Institute of Graphic Communication  
Beijing 102600, P. R. China

Y. Feng, J. An, X. Liang, Prof. T. Jiang, Prof. Z. L. Wang  
School of Nanoscience and Technology  
University of Chinese Academy of Sciences  
Beijing 100049, P. R. China  
Prof. T. Jiang, Prof. Z. L. Wang  
CUSPEA Institute of Technology  
Wenzhou, Zhejiang 325024, P. R. China  
Prof. Z. L. Wang  
School of Materials Science and Engineering  
Georgia Institute of Technology  
Atlanta, GA 30332-0245, USA

 The ORCID identification number(s) for the author(s) of this article can be found under <https://doi.org/10.1002/admt.202100496>.

DOI: 10.1002/admt.202100496

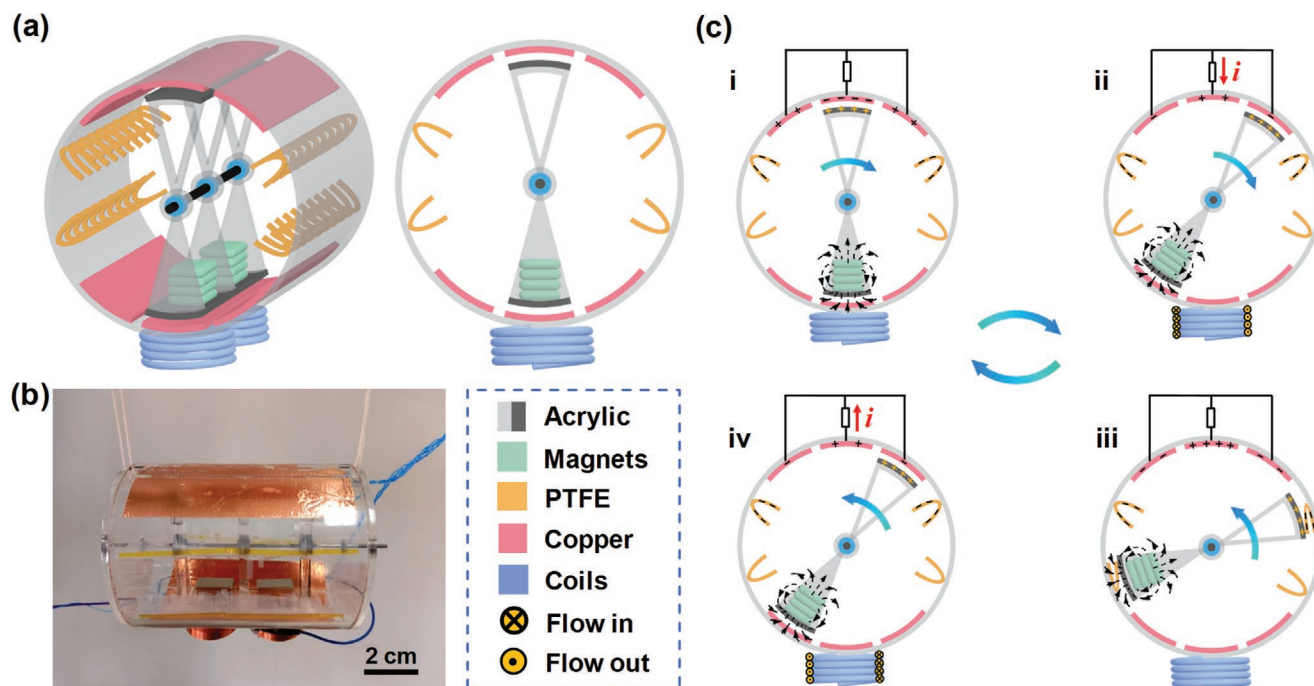


**Figure 1.** a) Schematic representation of the swing-structured triboelectric–electromagnetic hybrid nanogenerator, including the 3D structure and cross-section view. b) Photograph of the fabricated hybrid TENG/EMG device. c) Schematic illustration for the working principle of the hybrid nanogenerator.

low-frequency energy, such as water wave energy and wind energy.<sup>[15–17]</sup> Although the two technologies are quite different in structure and principle, they are complementary rather than mutually substituted in practical applications for wider frequency range and better performance.<sup>[18]</sup> Recently, several prototypes of triboelectric-electromagnetic hybrid nanogenerators have been developed to effectively harvest mechanical energy.<sup>[19–27]</sup> However, the output characteristics of the two generators were not systematically compared with each other. A common character is that their output characteristics were compared under a circumstance of non-rectification, and the outputs of EMG are higher than those of TENG. However, usually the translated electric energy from TENG or EMG needs to be rectified for powering electronics or storage. Due to the existence of the threshold voltage for the rectifying component, the rectified outputs for the TENG and EMG may be much different. Therefore, it is very necessary to reveal the individual and combined characteristics of the two generators in the hybrid device. In previous works, a kind of swing-structured TENG (SS-TENG), which possesses high energy conversion efficiency and strong durability, was proposed to harvest the water wave energy and wind energy,<sup>[28–30]</sup> followed by a hybrid TENG/EMG structure for water wave energy harvesting.<sup>[31]</sup> The application of such swing-structured hybrid device in capturing the breeze wind energy needs to be further demonstrated.

In the present work, a swing-structured hybrid nanogenerator made of cylindrical TENG and EMG was designed for harvesting breeze wind energy. Flexible dielectric brushes and air gaps between triboelectric layers and electrodes were adopted to enhance the device robustness and durability due to the minimized frictional resistance and continuous supply of triboelectric charges. First, the ability of pure SS-TENG in

harvesting the breeze wind energy was demonstrated. Based on this, the TENG was hybridized with EMG to further improve its performance by attaching two coils underneath the TENG shell and replacing the mass blocks by magnets. The output and charging characteristics of the hybrid TENG/EMG device were then systematically investigated under regular external triggering conditions. Importantly, the rectified output performance for the TENG part and EMG part was compared, and the influences of the air gap and turn number of coils (diameter: 0.1 mm) were addressed. Moreover, under the breeze triggering, the performance of the hybrid nanogenerator and array device hung on tree branches with respect to the wind speed was revealed, and a wireless transmitter was successfully powered by the hybrid array for application of self-powered environmental monitoring.

## 2. Results and Discussion

A schematic diagram of designed hybrid TENG/EMG device is shown in **Figure 1a**, including the 3D structure and cross-section view. The structure of hybrid nanogenerator is based on the swing-structured TENG reported previously,<sup>[29]</sup> whose schematic representation can also be seen in Figure S1, Supporting Information. The SS-TENG uses a steel shaft to connect three bearing-enclosed swing acrylic connected-sectors, which are adhered together by two arc-shaped acrylic strips with a central angle of 30°, and two circular acrylic disks on both ends. Several copper blocks are added onto the bottom arc-shaped strip to lower the center of gravity. Four groups of polytetrafluoroethylene (PTFE) strips and six copper electrodes are attached onto the internal wall of the outer acrylic shell. There is an air gap

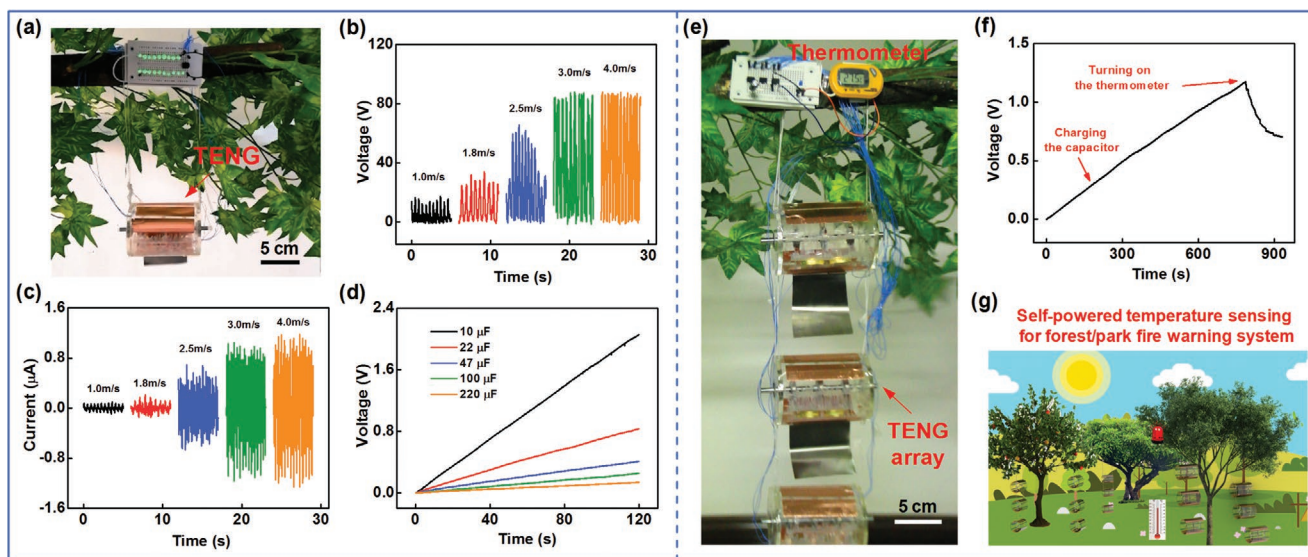


**Figure 2.** a) Photograph of twenty LEDs lighted up by a SS–TENG device hung on a tree branch under the breeze wind triggering. Influence of the wind speed on the b) output voltage and c) output current of the SS–TENG device. d) Charging voltage on various capacitances for the TENG at the wind speed of  $4.0 \text{ m s}^{-1}$ . e) Photograph of a digital thermometer powered by a SS–TENG array under the wind triggering. f) Charging and discharging processes for a capacitor of  $470 \text{ }\mu\text{F}$  to power the thermometer. g) Schematic illustration of the self-powered temperature sensing for forest/park fire warning system based on the SS–TENG array.

existing between the arc-shaped acrylic strip surface and the electrodes. The PTFE brushes can supply the triboelectric charges during the contact/separation with the arc-shaped acrylic surfaces. Then, based on the SS–TENG, the copper mass blocks are replaced by rectangular magnets, which are magnetized along the thickness direction and stacked from bottom to top. And two coils are installed onto the bottom external wall of TENG shell, forming a hybrid TENG/EMG device. The detailed fabrication process can be found in the Experimental Section. Figure 1b shows a photograph of the fabricated hybrid TENG/EMG device.

The working principle of the hybrid nanogenerator is schematically presented in Figure 1c. For the TENG part, as described previously, two processes exist, that is, triboelectrification process and electrostatic induction. When the swing component swings to contact with the PTFE strips (with pre-injected electrons) under an external triggering, the triboelectrification between PTFE and acrylic surface occurs, generating opposite electrostatic charges on their surfaces, which get saturated after several cycles. As shown from the TENG top in Figure 1c, two freestanding TENGs are connected in parallel with a shared middle electrode. There are equal amounts of opposite charges on the middle and left/right electrodes at the initial state (Figure 1c-i). The electrons flow from the middle electrode to the left/right electrodes through the external circuit, when the swing component moves rightward under a triggering (Figure 1c-ii). The induced current is generated until the maximum swing amplitude (Figure 1c-iii). Then a backward swing of the swing component will produce a reversed induced current across the external load (Figure 1c-iv). The low frictional resistance between the acrylic surfaces and PTFE and non-contact electrostatic induction process make the TENG possess good device durability. The detailed description for the working principle of SS–TENG can be seen from our previous work.<sup>[29]</sup> For the EMG part, the generation mechanism is based on the

electromagnetic induction. When the magnets adhered on the bottom arc-shaped acrylic strip swings back and forth above the two coils connected in series, the closed coils cut the magnetic flux lines, and the magnetic flux through the coils changes. As a result, intense current is induced in the Cu coils made of wires with a diameter of  $0.1 \text{ mm}$ , whose direction is dependent on the swing direction. Assuming the top of the magnet is its N pole, the current direction in the coils can be judged by Lenz's law.

First, before investigating the performance of hybrid nanogenerator, we demonstrated the ability of SS–TENG device in harvesting breeze wind energy, which is a subsequent study based on the previous work of SS–TENG for blue energy harvesting.<sup>[29]</sup> A SS–TENG with smaller size was fabricated to be hung on a tree branch, as shown in Figure 2a. Under the breeze blows, twenty LEDs can be lighted up by the TENG (Video S1, Supporting Information). Note that when we applied the wind at a specific wind speed, the wind direction is continually changing to make the TENG work well. A flap was also used to capture the wind, facilitating the motion of TENG device. Then the electric outputs of the TENG at different wind speeds simulated by the transient wind were measured, as shown in Figure 2b,c; Figure S2a, Supporting Information. The output current, voltage, and charge all first increase and finally get saturated with increasing the wind speed. The SS–TENG is sensitive to the wind speed and can work at the breeze blow. The charging profiles for different capacitors in Figure 2d show that the output charge reaches  $30.8 \text{ }\mu\text{C}$  for the capacitor of  $220 \text{ }\mu\text{F}$  within  $120 \text{ s}$  under the wind triggering. Then we fabricated the SS–TENG array by connecting three units in parallel and then hung it on the tree branch to harvest the breeze wind energy, as shown in Figure 2e. The output current is presented in Figure S2b, Supporting Information. A digital thermometer was successfully powered by the TENG array under the wind triggering as an application demonstration (Video S2, Supporting

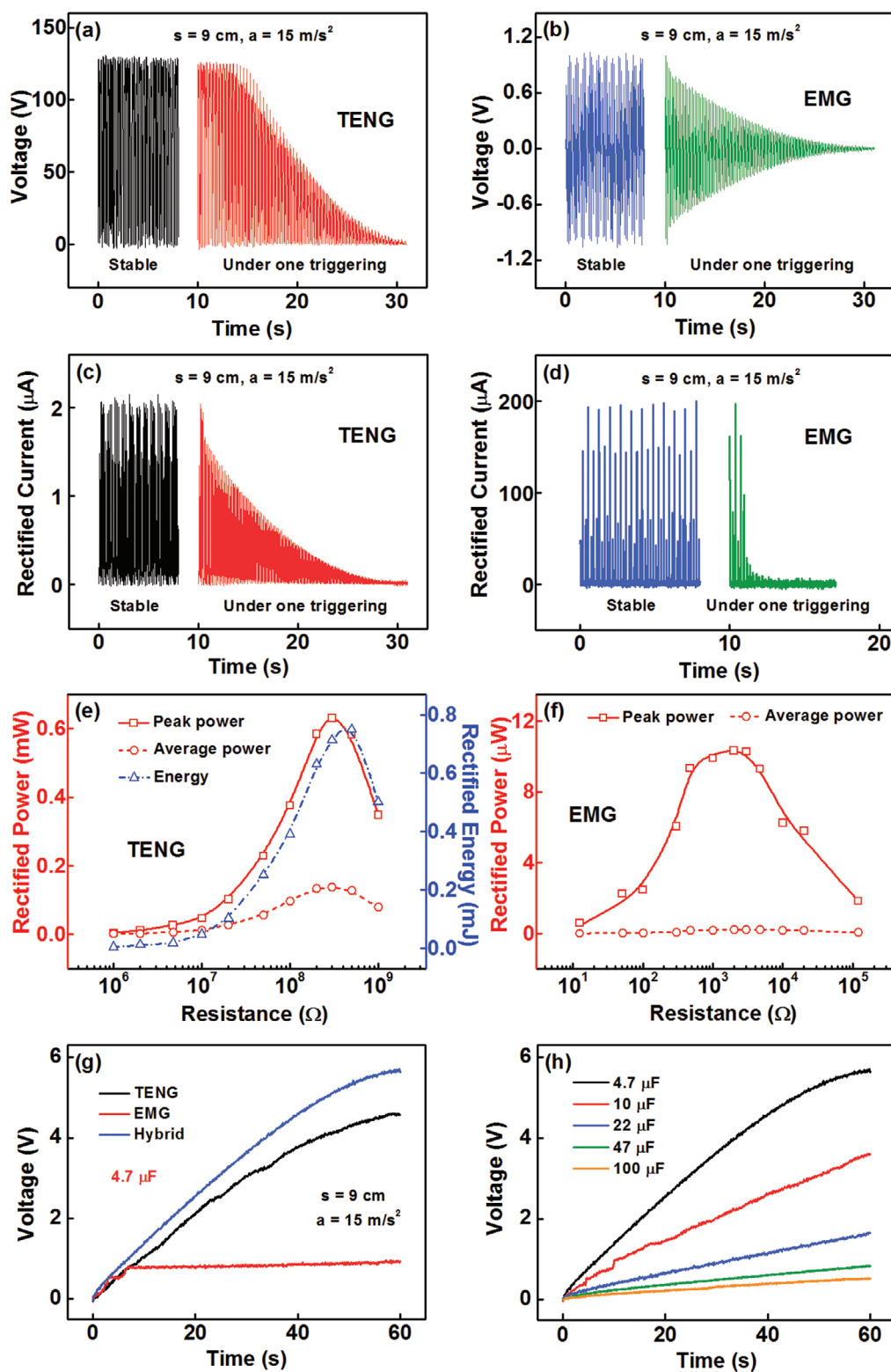


**Figure 3.** Output voltage of the a) TENG part and b) EMG part in the hybrid nanogenerator under stable triggering and one triggering of linear motor. The motor parameters for applying the triggering are  $s = 9$  cm and  $a = 15$  m/s<sup>2</sup>. Rectified output current of the c) TENG part and d) EMG part of the hybrid nanogenerator under stable triggering and one triggering. e) Rectified peak output power, rectified average output power–resistance relationships under stable triggering at  $s = 9$  cm and  $a = 15$  m/s<sup>2</sup> and rectified translated energy–resistance relationship under one triggering for the TENG part. f) Rectified peak power and average power with respect to the load resistance for the EMG part. g) Comparison of charging a capacitor of 4.7 µF for the TENG, EMG, and the hybrid nanogenerator. h) Charging voltage on various capacitances for the hybrid nanogenerator.

Information). The corresponding voltage profile in the charging and discharging processes is shown in Figure 2f, indicating that the thermometer can work for more than 1 min after charging the capacitor of 470  $\mu\text{F}$  to 1.2 V. The TENG array can detect the environment temperature by harvesting the breeze wind energy, which will have important applications in forest/park fire warning. If the temperature exceeds the set warning value, an alarm will work and send out sound and light. A schematic self-powered forest/park fire warning system constructed based on the SS-TENG arrays hung on the tree branches through the temperature sensing is shown in Figure 2g.

Based on the result that the SS-TENG exhibits good ability in harvesting breeze wind energy, we systematically evaluated the performance of as-fabricated hybrid nanogenerator consisting of SS-TENG and EMG. The output characteristics of the TENG part and EMG part under a regular triggering were compared, with focus on the rectified output performance, as shown in Figure 3. The motor acceleration and maximum displacement were set as  $a = 15 \text{ m s}^{-2}$  and  $s = 9 \text{ cm}$ . A hybrid nanogenerator with an air gap of  $g = 1 \text{ mm}$  between the acrylic surfaces and electrodes and a turn number  $n = 2700$  of each coil was taken for example. As shown in Figure 3a,c, the TENG part can generate a maximum output voltage of 129 V and a maximum rectified current of 2.1  $\mu\text{A}$  under stable triggering. Due to the damping oscillation of the swing component after one triggering, the voltage and rectified current both attenuate gradually to zero, as well as the output current and transferred charge without rectification (Figure S3a, c, Supporting Information). Compared to the output current without rectification, the rectified current through a rectifier bridge (DB107) has a slight change. There is a short initial plateau for the charge profile, because the swing amplitude can be beyond all the Cu electrodes. Figure 3b,d shows the maximum output voltage and rectified current of the EMG parts are 1.0 V and 196  $\mu\text{A}$ . Although the rectified current of EMG is larger than that of TENG, the current after rectification exhibits a significant decrease in contrast to the output current of 2.0 mA (Figure S3b, Supporting Information), due to the existence of the rectifier bridge, and also the damping behavior is not good. The output voltage of EMG is low so that the threshold voltage required for the rectifier bridge can largely reduce the effective power output by EMG. However, for TENG, its output voltage is high, so that the voltage consumed at the rectifier bridge makes little impact to the effective power output. This is why the TENG is much more effective than EMG for harvesting energy from low frequency motion.

The output behaviors of the TENG part and EMG part when loading a resistor before and after the rectification were respectively studied, as shown in Figure 3e,f; Figure S3d,e, Supporting Information. The rectified peak output power, rectified average output power–resistance relationships under stable triggering at  $s = 9 \text{ cm}$  and  $a = 15 \text{ m s}^{-2}$  and rectified translated energy–resistance relationship under one triggering for the TENG part are presented in Figure 3e. As can be seen, the TENG can deliver the maximum rectified peak power of 0.63 mW at a matched resistance of 300  $\text{M}\Omega$ , rectified average power of 0.14 mW at 300  $\text{M}\Omega$ , and the maximum rectified energy of 0.75 mJ at 500  $\text{M}\Omega$ . The corresponding rectified peak and average power densities are respectively, 1.25 and 0.28  $\text{W m}^{-3}$ .

The power and energy of TENG part without rectification are almost the same (Figure S3d, Supporting Information). On the other hand, the EMG part can achieve lower rectified output performance, with a rectified peak power of 10.32  $\mu\text{W}$  and rectified average power of 0.22  $\mu\text{W}$  at 2  $\text{k}\Omega$  (Figure 3f). The rectified energy cannot be calculated and is not shown, because the damping behavior is not obvious when loading a resistor and the rectified current cannot be captured after one triggering. Different from the TENG, after the rectification, the output performance of EMG has a significant decrease, relative to the higher outputs before the rectification (peak power of 0.57 mW, average power of 0.11 mW, and energy of 0.40 mJ, Figure S3e, Supporting Information). Concluding, in the current hybrid nanogenerator, the rectified peak power and average power of TENG part are 60 and 635 times, respectively, higher than those of EMG part. The results imply the great advantage of TENG over EMG in practical applications, because the electric energies are usually required to be rectified for storage or powering electronics.

Then, we studied the charging performance of the hybrid nanogenerator to commercial capacitors. A comparison of the charging voltage profile to a 4.7  $\mu\text{F}$  capacitor for the TENG part, EMG part, and the hybrid nanogenerator was made, as shown in Figure 3g. The charging voltage for the EMG increases and gets saturated in a short time, while the charging voltage for the TENG can increase gradually. And the charging speed for the hybrid nanogenerator is higher than that of both the TENG and EMG. The charging voltage profiles of the hybrid nanogenerator to various capacitors are shown in Figure 3h, indicating the good charging capability under the external triggering. The capacitor of 4.7  $\mu\text{F}$  can be charged to 5.7 V within 60 s, while 0.52 V for the 100  $\mu\text{F}$  capacitor, which corresponds to a stored charge amount of 52  $\mu\text{C}$ .

The air gap  $g$  between the triboelectric surfaces and electrodes and the turn number  $n$  of each coil are two important structural parameters influencing the performance of the hybrid TENG/EMG device. Figure 4a,b shows the output voltage and rectified output current of the TENG part for various air gaps, at fixed coil turn number of  $n = 2700$ . As the air gap increases from 1 to 5 mm, the voltage and rectified current both decrease gradually. The drop in the outputs is ascribed to the hindered charge transfer at larger air gap (Figure S4a, Supporting Information), and weaker electrostatic induction effect. The rectified peak power and average power under stable triggering and rectified energy under one triggering for the TENG part, as functions of the air gap, were also evaluated, as shown in Figure 4c. Obviously, the rectified peak power, rectified average power, and rectified energy all decrease with the air gap. When the air gap increases to 5 mm, they become only 0.06 mW, 0.01 mW, and 0.04 mJ, respectively. The inset indicates the maximum rectified peak power of the EMG part also decreases with the increase in air gap, which is ascribed to the increased distance between magnets and coils and weakened magnetic fields at the coils. The same reason makes the voltage and rectified current of EMG part both descend with the air gap (Figure S4b,c, Supporting Information). At  $g = 5 \text{ mm}$ , the rectified current of EMG part almost becomes zero, because the voltage of EMG is close to the threshold voltage of the rectifier bridge. In addition, when charging the 4.7  $\mu\text{F}$  capacitor, the smaller the air gap, the higher the charging speed for the hybrid nanogenerator.

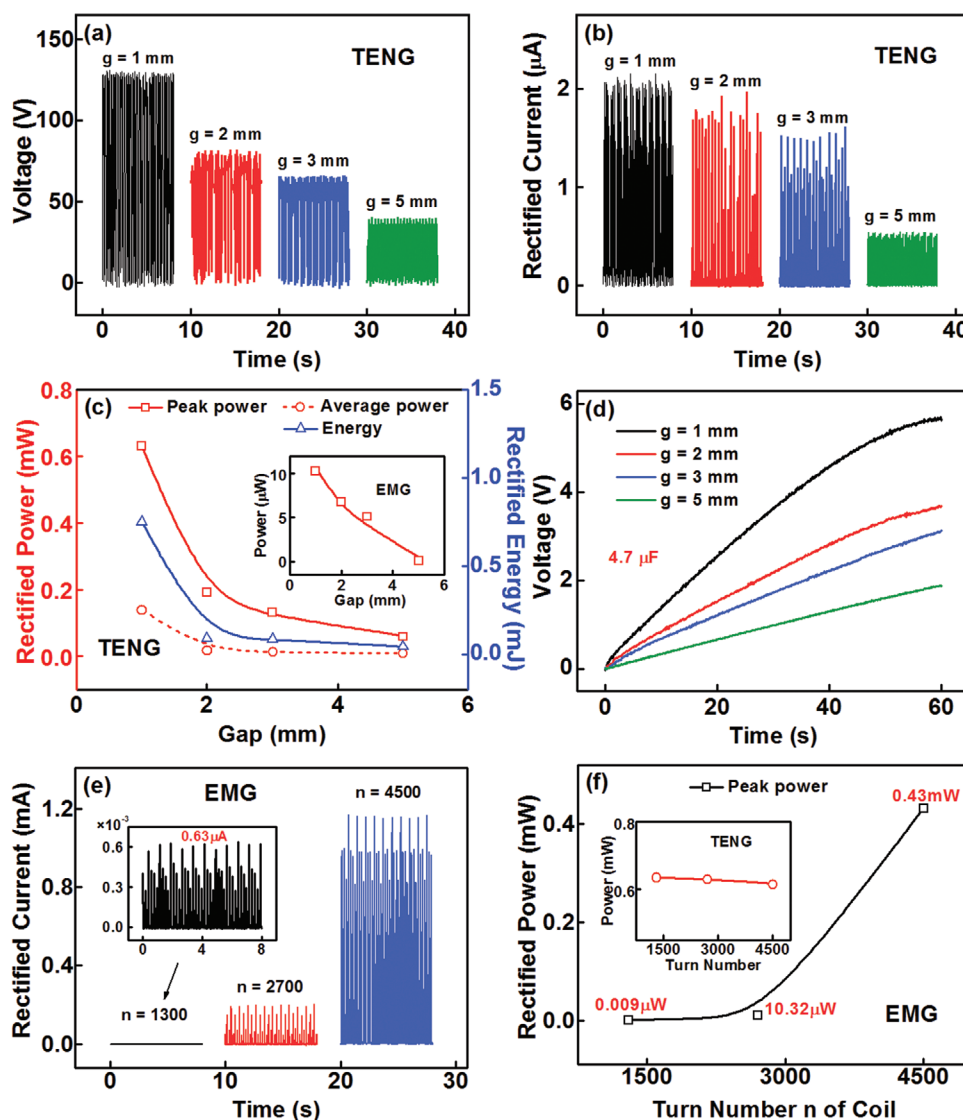


**Figure 4.** Influence of the air gap  $g$  between triboelectric layers and electrodes on the a) output voltage and b) rectified output current of the TENG part in the hybrid device at  $s = 9$  cm and  $a = 15$  m s<sup>-2</sup>. c) Maximum values of rectified peak power, rectified average power under stable triggering, and rectified energy under one triggering as functions of the air gap for the TENG part. The inset shows the maximum rectified peak power of the EMG part with the air gap. d) Comparison of the charging profiles for the hybrid nanogenerators with various air gaps. A capacitor of 4.7  $\mu$ F is chosen. e) Effect of the turn number  $n$  of each coil on the rectified current of the EMG part. An enlarged view of the rectified current profile for  $n = 1300$  is also shown. f) Maximum rectified peak power of the EMG part with respect to the turn number  $n$ , as well as the maximum rectified peak power of the TENG part.

Regarding the effects of the coil turn number, we employed three types of coil groups (two coils in series) with the turn number  $n$  of 1300, 2700, and 4500 to obtain the hybrid nanogenerator devices. The measured resistance of one coil is respectively, 110, 240, and 419  $\Omega$ , for the three types of coils. The rectified current and rectified peak power of the EMG part with respect to the turn number of coils are shown in Figure 4e,f. The rectified current and rectified peak power both exhibit an increasing tendency as the turn number of coils increases. At  $n = 1300$ , the rectified current is only 0.63  $\mu$ A, and the maximum rectified power is only 0.009  $\mu$ W. Such low rectified performance is attributed to the very low voltage of EMG (Figure S5a, Supporting Information). When the turn number

$n$  increases to 4500, the rectified current increases significantly to 1.2 mA, and the rectified peak power reaches 0.43 mW, due to the highest voltage of 2.4 V. However, for the TENG part, the turn number of coils was found to almost have no influence on the voltage, rectified current and rectified power, as shown in Figure 4f; Figure S5b,c, Supporting Information. In addition, for the EMG part with fixed coil volume, a smaller wire diameter  $d_w$  of the coils was found to be favorable to the rectified output performance of the EMG, because the increase in wire diameter will greatly decrease the output voltage (see Figure S6 and Notes in Supporting Information).

After revealing the performance of hybrid device under the regular triggering, the device was then hung on a tree branch

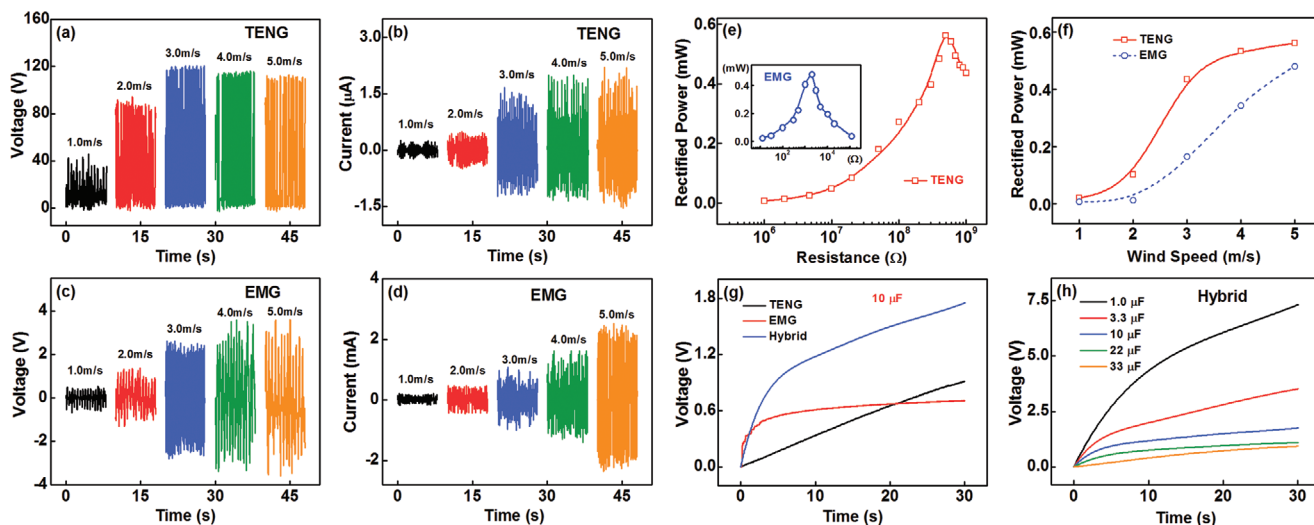


**Figure 5.** a) Output voltage and b) output current of the TENG part in single hybrid nanogenerator hung on a tree branch at different wind speeds. c) Output voltage and d) output current of the EMG part in single hybrid nanogenerator at different wind speeds. e) Rectified peak power–resistance relationships of the TENG part and EMG part in single hybrid nanogenerator under the wind triggering at the speed of  $5.0 \text{ m s}^{-1}$ . f) Maximum rectified peak power with respect to the wind speed for the TENG part and EMG part in single hybrid device. g) Comparison of the charging profiles of a  $10 \mu\text{F}$  capacitor for the TENG, EMG, and hybrid nanogenerator at the wind speed of  $5.0 \text{ m s}^{-1}$ . h) Charging voltage on various capacitances for single hybrid nanogenerator.

to harvest the real breeze wind energy. The simulated wind with different wind speeds was obtained by a blower, and the influence of the wind speed on the output and charging characteristics of single hybrid TENG/EMG device was investigated, as shown in **Figure 5**. To achieve better performance, the coils with  $n = 4500$  were chosen, and the air gap was 1 mm. The smaller total device weight makes the hybrid device effectively driven by the breeze wind without the assistance of a flap. And the adding of a flap can also affect the output performance of the EMG. So the flap was cancelled in the hybrid TENG/EMG structure. As the wind speed increases from  $1.0$  to  $5.0 \text{ m s}^{-1}$ , the output voltage and current of the TENG part both first increase and finally get nearly saturated (even a slight decrease for the voltage), as presented in **Figure 5a,b**. The first increase is due to the increase of swing amplitude until saturation with increasing the wind speed. And the drop of the voltage at higher wind speed is because the movement of the internal swing component is hindered by the rapidly moving cylindrical shell driven by the wind. By contrast, in the performed wind speed range, both the output voltage and current of the EMG part have a gradual increase with the wind speed (**Figure 5c,d**), because the induced electrodynamic potential is dependent on the angular frequency.

The resistive load behaviors for the TENG part and EMG part in the single hybrid nanogenerator under the wind triggering of  $5.0 \text{ m s}^{-1}$  were explored. It can be seen from **Figure 5e** that the rectified peak power of the TENG part and EMG part can reach  $0.56$  and  $0.48 \text{ mW}$ , respectively. The matched resistance for the TENG part and EMG part are respectively,  $500 \text{ M}\Omega$  and  $2 \text{ k}\Omega$ . Due to the great difference in the matched resistance, the TENG and EMG can power two different loads alone, with a total rectified peak power of  $1.04 \text{ mW}$  and a power density of  $2.07 \text{ W m}^{-3}$ . And the relationship between the rectified peak power and the wind speed indicates that the rectified peak

power of the TENG part increases with the wind speed until saturation, while that of the EMG part elevates gradually in the current wind speed range (**Figure 5f**). In addition, the charging performance of the hybrid device under the breeze triggering was measured. The results indicate that the charging speed of the hybrid nanogenerator is the highest among the TENG part, EMG part, and hybrid device (for  $10 \mu\text{F}$  capacitor, **Figure 5g**). **Figure 5h** shows the charging voltage on various capacitances for the hybrid nanogenerator. The voltage of the  $33 \mu\text{F}$  capacitor can be raised to  $0.93 \text{ V}$  within  $30 \text{ s}$  with a stored charge of  $30.7 \mu\text{C}$  by the hybrid device under the wind triggering. For the TENG part, the charging voltage on different capacitors has a nearly linear increase within  $30 \text{ s}$ , but it gets saturated rapidly for the EMG part (**Figure S7**, Supporting Information).

Subsequently, we integrated three such hybrid nanogenerator units into a hybrid array device by connecting them in parallel. The rectified output performance of the hybrid TENG/EMG array hung on the tree branch was measured when applying the breeze triggering at the wind speed of  $5.0 \text{ m s}^{-1}$ , as depicted in **Figure 6a,b**. The maximum rectified current of the TENG part and EMG part can reach  $4.1 \mu\text{A}$  and  $3.3 \text{ mA}$ , respectively. The TENG part and EMG part were found to generate the rectified peak power of  $1.57$  and  $1.36 \text{ mW}$  at the matched resistances, as shown in **Figure 6b**. According to the total volume of three hybrid units, the rectified power density of the hybrid array was calculated to be  $1.94 \text{ W m}^{-3}$ .

Finally, the application of the hybrid TENG/EMG array device in self-powered environmental monitoring by wind energy harvesting was demonstrated. The wind condition with a speed of  $5.0 \text{ m s}^{-1}$  was fixed. **Figure 6c** shows the charging performance of the fabricated hybrid array to various capacitors. At the initial stage of the charging process, the charging speed is rapid due to the existence of the EMGs, and then decreases with the charging time. Also, with increasing the

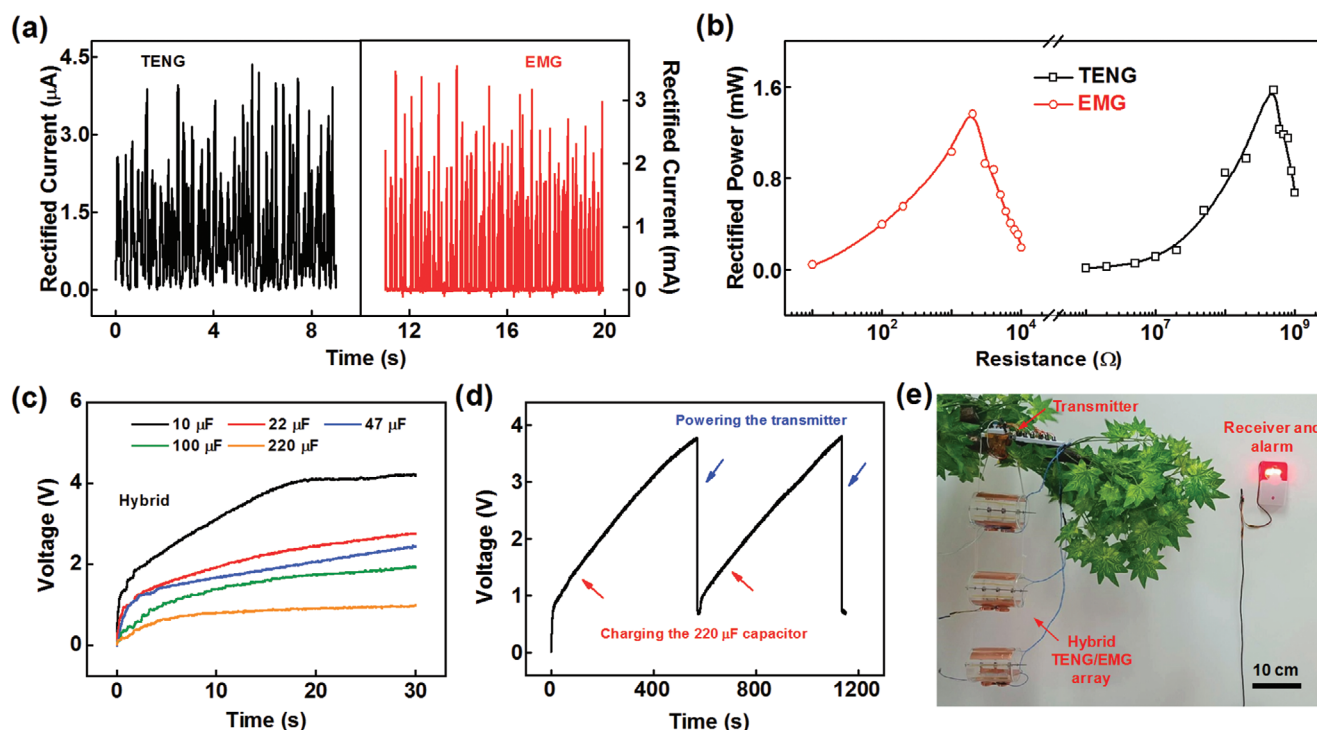


**Figure 6.** a) Rectified output current of the TENG part and EMG part for a hybrid TENG/EMG array hung on a tree branch at the wind speed of  $5.0 \text{ m s}^{-1}$ . b) Rectified peak power of the TENG part and EMG part with respect to the load resistance for the hybrid TENG/EMG array under the wind triggering. c) Charging voltage on various capacitances for the hybrid TENG/EMG array device. d) Charging and discharging voltage on a  $220 \mu\text{F}$  capacitor when powering a wireless transmitter by the hybrid array for two consequent cycles. e) Photograph of the transmitter powered by the hybrid array under the wind triggering, where the transmitter sends a signal to the receiver for alarm.

capacitance, the charging speed decreases. For the capacitor of  $10 \mu\text{F}$ , the charge amount of  $42.2 \mu\text{C}$  can be stored in 30 s, while the stored charge reaches  $218.8 \mu\text{C}$  for the capacitor of  $220 \mu\text{F}$ . Then, the  $220 \mu\text{F}$  capacitor was chosen to store the translated electric energy for powering a wireless transmitter. The charging voltage on the capacitor during the charging–discharging process is shown in Figure 6d. The photograph in Figure 6e; Video S3, Supporting Information, shows the transmitter was successfully powered by the wind driven hybrid array to send a signal to the receiver for sound and light alarming. The transmission distance can be above 10 m, but the case with the distance of  $\approx 1 \text{ m}$  is shown due to the space limitation. When the  $220 \mu\text{F}$  capacitor was charged to  $\approx 3.7 \text{ V}$  in  $\approx 9 \text{ min}$ , the transmitter was connected to send the signal by closing the switch. The charging time for the next cycle was still  $\approx 9 \text{ min}$  due to the rapid charging speed at the initial stage. The successful powering of the wireless transmitter demonstrates important applications of the hybrid TENG/EMG array triggered by distributed breezes in self-powered environmental monitoring for forest/park fire warning system.

In this work, we want to systematically compare the output characteristics of TENG and EMG after the rectification and further improve the harvesting capacity of breeze wind energy at certain volume through the combination of the two generators. We found that the rectified peak power and average power of TENG part are much higher than those of EMG part at moderate coil turn numbers, which is one of the main innovative findings of this work. Besides, the swing device structure

is very suitable to be arrayed and hung on tree branches to harvest the breeze wind energy, having important applications in self-powered forest/park fire warning, especially in the desert regions. Also the combination of the TENG with EMG can further improve the capacity of the device in wind energy harvesting, including the enhanced output power density of device and widened wind speed/frequency range that can be harvested.

### 3. Conclusion

In summary, a robust swing-structured hybrid TENG/EMG device with enhanced device durability was fabricated to harvest low-frequency breeze wind energy. After revealing the capability of pure SS–TENG in breeze wind energy harvesting for self-powered applications, the output and charging performance of the hybrid nanogenerator were studied under external triggering, with focus on the comparison of the performance for the TENG part and EMG part. The rectified peak power and average power of TENG part exhibit 60 and 635 times, respectively, higher than those of EMG part at a moderate turn number of coils, indicating the obvious advantages of TENG in practical applications. The output performance of the hybrid device was also found to be controlled by the air gap and coil turn number. Furthermore, the single hybrid nanogenerator and hybrid TENG/EMG array were applied to harvest the breeze wind energy with different wind speeds, generating total

rectified peak power densities of  $2.07 \text{ W m}^{-3}$  and  $1.94 \text{ W m}^{-3}$  for the single and array devices, respectively. Portable electronics were successfully powered to show potential applications of the hybrid nanogenerators in self-powered environmental monitoring and forest/park fire warning.

## 4. Experimental Section

*Fabrications of the SS-TENG Device and Hybrid TENG/EMG Device:* First, a SS-TENG with two cylindrical copper mass blocks adhered on bottom arc-shaped acrylic strip was fabricated. Similar to the previous work,<sup>[29]</sup> a steel shaft with a diameter of 6 mm was used to support three commercial bearings (inner diameter: 6 mm, outer diameter: 17 mm), which were embedded into three connected-sector acrylic blocks with holes of 17 mm. The arc-shaped acrylic strips were prepared by dividing a cylindrical shell (length: 8 cm, outer diameter: 7 cm, thickness: 2 mm) into 12 equal pieces. The acrylic shell of TENG had a length of 10 cm, a thickness of 3 mm, and an outer diameter of 8 cm. Six Cu electrodes and four groups of PTFE strips were attached onto the internal wall of the shell. The pre-injection time of the electrons onto the surface of PTFE was 6 min at a polarization voltage of 5 kV. After sealing the acrylic shell, the SS-TENG device was obtained, followed by the fabrication of SS-TENG array by connecting three TENG units in a parallel manner. When harvesting the breeze wind energy, a folded flap made of a rigid stainless steel blade (7.5 cm × 6 cm) with sharp edges was adhered onto the outside shell of each TENG to facilitate the motion of TENG device for more effective energy capturing, due to the larger device weight.

Then, for the hybrid TENG/EMG device, a steel shaft with a smaller diameter of 2 mm and smaller bearings (inner diameter: 2 mm, outer diameter: 6 mm) was adopted, considering the total device weight after adding the coils. The air gap between the acrylic surfaces and electrodes was adjusted by using different sizes of connected-sector acrylic blocks (with holes of 6 mm). Two groups of four stacked rectangular magnets, magnetized along the thickness direction, were attached onto the arc-shaped acrylic strips between adjacent connected-sectors to replace the initial copper blocks. Each sintered neodymium-iron-boron (NdFeB) magnet, coated with nickel, had a size of 20 mm × 10 mm × 2 mm and a weight of 3.7 g. Two coils with variable turn number, just below the magnets, were adhered onto the bottom external wall of TENG shell. Three types of coils with the same wire diameter of 0.1 mm and inner diameter of 5 mm, had different outer diameters and thicknesses: 2 cm, 2.5 mm; 2 cm, 5 mm; 3 cm, 5 mm. The corresponding turn numbers for each coil were respectively, 1300, 2700, and 4500. When studying the effect of the wire diameter, the volume of the coils was fixed, so the turn number was variable. The outer diameter, inner diameter, and thickness of the two adopted coils were respectively 30, 5, and 5 mm. Finally, a hybrid TENG/EMG array device was fabricated through integrating three units by flexible strings, and was hung on tree branches for harvesting breeze wind energy.

*Electric Measurements of the TENG Part, EMG Part, and the Hybrid Device:* The electrical output signals of the TENG part, EMG part, and the hybrid device were measured under the ideal triggering generated by a linear motor or under the wind blow triggering. The speed of the wind generated by a blower was measured by an anemometer, which was changed by adjusting the blower gear for studying its effect on the outputs. The output current, voltage, and transferred charge of the TENG part, EMG part, and the hybrid device, and charging voltage on capacitors were all measured by a current preamplifier (Keithley 6514 System Electrometer).

## Supporting Information

Supporting Information is available from the Wiley Online Library or from the author.

## Acknowledgements

P.L. and H.P. contributed equally to this work. Support from the National Key R & D Project from Minister of Science and Technology (2016YFA0202704), National Natural Science Foundation of China (Grant Nos. 51432005, 51702018, and 51561145021), and Youth Innovation Promotion Association, CAS, are appreciated.

## Conflict of Interest

The authors declare no conflict of interest.

## Data Availability Statement

Research data are not shared.

## Keywords

breeze wind energy harvesting, self-powered environmental monitoring, swing structure, triboelectric–electromagnetic hybrid nanogenerator

Received: April 27, 2021

Published online:

- [1] J. P. Painuly, *Renewable Energy* **2001**, *24*, 73.
- [2] W. El-Khattam, M. M. A. Salama, *Electr. Power Syst. Res.* **2004**, *71*, 119.
- [3] Z. L. Wang, *Nano Energy* **2019**, *58*, 669.
- [4] Z. Wang, W. Zhao, S. Hu, A. Xu, Q. Jiang, H. Jiang, S. Huang, Q. Li, *Nat. Gas Ind. B* **2017**, *4*, 141.
- [5] S. P. Beeby, M. J. Tudor, N. M. White, *Meas. Sci. Technol.* **2006**, *17*, R175.
- [6] B. Chen, Y. Yang, Z. L. Wang, *Adv. Energy Mater.* **2018**, *8*, 1702649.
- [7] P. Devine-Wright, *Wind Energy* **2005**, *8*, 125.
- [8] R. Hallali, F. Dalaudier, J. Parent du Chatelet, *Boundary-Layer Meteorol.* **2016**, *160*, 299.
- [9] M. Free, B. Sun, H. L. Yoo, *J. Clim.* **2016**, *29*, 2015.
- [10] F. R. Fan, Z. Q. Tian, Z. L. Wang, *Nano Energy* **2012**, *1*, 328.
- [11] J. Chen, H. Guo, C. Hu, Z. L. Wang, *Adv. Energy Mater.* **2020**, *10*, 2000886.
- [12] Z. L. Wang, *Adv. Energy Mater.* **2020**, *10*, 2000137.
- [13] Z. L. Wang, *Mater. Today* **2017**, *20*, 74.
- [14] J. Zhao, G. Zhen, G. Liu, T. Bu, W. Liu, X. Fu, P. Zhang, C. Zhang, Z. L. Wang, *Nano Energy* **2019**, *61*, 111.
- [15] Z. L. Wang, T. Jiang, L. Xu, *Nano Energy* **2017**, *39*, 9.
- [16] C. Wu, A. C. Wang, W. Ding, H. Guo, Z. L. Wang, *Adv. Energy Mater.* **2019**, *9*, 1802906.
- [17] Q. Zeng, Y. Wu, Q. Tang, W. Liu, J. Wu, Y. Zhang, G. Yin, H. Yang, S. Yuan, D. Tan, C. Hu, X. Wang, *Nano Energy* **2020**, *70*, 104524.
- [18] C. Zhang, W. Tang, C. Han, F. Fan, Z. L. Wang, *Adv. Mater.* **2014**, *26*, 3580.
- [19] V. Vivekananthan, A. Chandrasekhar, N. R. Alluri, Y. Purusothaman, G. Khandelwal, R. Pandey, S.-J. Kim, *Nano Energy* **2019**, *64*, 103926.
- [20] X. Fan, J. He, J. Mu, J. Qian, N. Zhang, C. Yang, X. Hou, W. Geng, X. Wang, X. Chou, *Nano Energy* **2020**, *68*, 104319.
- [21] L. Gao, S. Lu, W. Xie, X. Chen, L. Wu, T. Wang, A. Wang, C. Yue, D. Tong, W. Lei, H. Yu, X. He, X. Mu, Z. L. Wang, Y. Yang, *Nano Energy* **2020**, *72*, 104684.

- [22] J. Wan, H. Wang, L. Miao, X. Chen, Y. Song, H. Guo, C. Xu, Z. Ren, H. Zhang, *Nano Energy* **2020**, *74*, 104878.
- [23] Q. Han, Z. Ding, W. Sun, X. Xu, F. Chu, *Sustainable Energy Technol. Assess.* **2020**, *39*, 100717.
- [24] Y. Fang, T. Tang, Y. Li, C. Hou, F. Wen, Z. Yang, T. Chen, L. Sun, H. Liu, C. Lee, *iScience* **2021**, *24*, 102300.
- [25] C. Ye, K. Dong, J. An, J. Yi, X. Peng, C. Ning, Z. L. Wang, *ACS Energy Lett.* **2021**, *6*, 1443.
- [26] T. Quan, X. Wang, Z. L. Wang, Y. Yang, *ACS Nano* **2015**, *9*, 12301.
- [27] Y. Zhang, Q. Zeng, Y. Wu, J. Wu, S. Yuan, D. Tan, C. Hu, X. Wang, *Nano-Micro Lett.* **2020**, *12*, 175.
- [28] Z. Lin, B. Zhang, H. Guo, Z. Wu, H. Zou, J. Yang, Z. L. Wang, *Nano Energy* **2019**, *64*, 103908.
- [29] T. Jiang, H. Pang, J. An, P. J. Lu, Y. W. Feng, X. Liang, W. Zhong, Z. L. Wang, *Adv. Energy Mater.* **2020**, *10*, 2000064.
- [30] Y. Feng, T. Jiang, X. Liang, J. An, Z. L. Wang, *Appl. Phys. Rev.* **2020**, *7*, 021401.
- [31] Y. Feng, X. Liang, J. An, T. Jiang, Z. L. Wang, *Nano Energy* **2021**, *81*, 105625.